Optimization of EV and Green Source Fed Five-Level UPQC for Power Quality and Energy Management Using Fennec Fox Algorithm

Praveen Kumar Balachandran[1,2,3,*], Gudikandhula Kalpana[4], Vadla Babyshalini[5], Koganti Srilakshmi[6] and Subhav Singh[7,8]

[1] Department of Electrical and Electronics Engineering, Vardhaman College of Engineering, Hyderabad, 501218, Telangana, India

[2] Department of Electrical and Electronics Engineering, Chennai Institute of Technology, Chennai, 600069, Tamilnadu, India

[3] Centre of Research Impact and Outcome, Chitkara University, Rajpura, 140417, Punjab, India

[4] Department of Computer Science Engineering, Malla Reddy Engineering College for Women, Hyderabad, 500014, Telangana, India

[5] Department of Electrical and Electronics Engineering, JNTUH University College of Engineering, Jagtial, 505501, Telangana, India

[6] Department of Electrical and Electronics Engineering, Sreenidhi Institute of Science and Technology, Hyderabad, 501301, Telangana, India

[7] Chitkara Centre for Research and Development, Chitkara University, Baddi, 174103, Himachal Pradesh, India

[8] Division of Research and Development, Lovely Professional University, Phagwara, 144411, Punjab, India

INFORMATION

Keywords:
Neural network controller
fennec fox optimization algorithm
power quality
comparative analysis

DOI: 10.23967/j.rimni.2025.10.66625

SCIPEDIA Revista Internacional de Métodos Numéricos para Cálculo y Diseño en Ingeniería

Revista Internacional Métodos numéricos para cálculo y diseño en ingeniería RIMNI CIMNE

Optimization of EV and Green Source Fed Five-Level UPQC for Power Quality and Energy Management Using Fennec Fox Algorithm

Praveen Kumar Balachandran[1,2,3,*], Gudikandhula Kalpana[4], Vadla Babyshalini[5], Koganti Srilakshmi[6] and Subhav Singh[7,8]

[1]Department of Electrical and Electronics Engineering, Vardhaman College of Engineering, Hyderabad, 501218, Telangana, India

[2]Department of Electrical and Electronics Engineering, Chennai Institute of Technology, Chennai, 600069, Tamilnadu, India

[3]Centre of Research Impact and Outcome, Chitkara University, Rajpura, 140417, Punjab, India

[4]Department of Computer Science Engineering, Malla Reddy Engineering College for Women, Hyderabad, 500014, Telangana, India

[5]Department of Electrical and Electronics Engineering, JNTUH University College of Engineering, Jagtial, 505501, Telangana, India

[6]Department of Electrical and Electronics Engineering, Sreenidhi Institute of Science and Technology, Hyderabad, 501301, Telangana, India

[7]Chitkara Centre for Research and Development, Chitkara University, Baddi, 174103, Himachal Pradesh, India

[8]Division of Research and Development, Lovely Professional University, Phagwara, 144411, Punjab, India

ABSTRACT

Distribution systems have been significantly impacted in the present scenario by incorporating solar and wind power electronic devices. This work designs the synchronous reference frame theory (SRFT) based five-level cascade H-bridge unified power quality conditioner (UPQC) by optimizing the weights and bias values of the neural network controller (NNC) and the filter parameters using the Fennec fox optimization algorithm (FFOA). The primary goal is to efficiently tackle the power quality difficulties, including voltage distortions, direct current (DC) link capacitor voltage (DLCV) balancing, and to reduce the source current total harmonic distortion (THD) of the system connected to the grid that integrates wind energy system (WES) and solar system, including electric vehicle (EVs) along with battery energy storage system (BESS) which is denoted as (5LU-SWBEV). The study also intends to use a Fuzzy logic controller (FLC) regulation to control the flow of power between the grid, battery storage, EV and renewable sources. However, this facilitates the management of power transfer between solar/wind/battery and the grid and between EVs and consumer loads. Additionally, this integration contributes to a consistent electricity supply, effective demand fulfillment, and efficient use of generated power. The study shows that the optimal UPQC combined with FLC-based power flow management can handle power quality (PQ) issues and accomplish suitable and efficient power sharing.

OPEN ACCESS

Received: 13/04/2025

Accepted: 09/06/2025

Published: 15/08/2025

DOI
10.23967/j.rimni.2025.10.66625

Keywords:
Neural network controller
fennec fox optimization algorithm
power quality
comparative analysis

*Correspondence: Praveen Kumar Balachandran (praveenbala038@gmail.com).

Abbreviations

PQ	Power quality
PIDC	Proportional integral derivate controller
RES	Renewable energy sources
EMVPA	Enhanced most valuable player algorithm
SPV	Solar photovoltaic
UPQC	Unified Power Quality Conditioner
WES	Wind energy systems
EVs	Electric vehicles
FACTS	Flexible Alternating Current Transmission Systems
ANFIS	Artificial neuro-fuzzy interface system
FL	Fuzzy logic
ANN	Artificial neural network
NNC	Neural network control
SVC	Static Var Compensator
BESS	Battery energy storage system
OCV	Open circuit voltage
THD	Total Harmonic Distortion
SOC	Short circuit current
DSTATCOM	Distribution Static Synchronous Compensator
DVR	Dynamic Voltage Restorer
GA	Genetic Algorithm
SHAPF	Shunt active power filters
ACO	Ant colony optimization
SOCOB	State of charge of battery
VSC	Voltage Source Converters
MSF	Membership Function
PSO	Particle swarm optimization
DLCV	DC Link capacitor Voltage
NOV	Nominal Voltage
PLL	Phase-Locked Loop
ST	Station
PWM	Pulse Width Modulation
V_{S_abc}	Source voltage for abc phases
i_{S_abc}	Source current for abc phases
i_{sh_abc}	Shunt filter supplied in abc phases
V_{l_abc}	Load voltage for phases abc
V_{se_abc}	Series injected voltage for phases a, b, c
$V^{ref}{}_{se\_dq}$	Reference voltage for the series converter in dq
$i^{ref}{}_{sh\_abc}$	Reference current injected for phases abc
V_{l_abc}	Load current for phases abc
R_{sh}, R_{se}, L_{sh}, L_{se}	Resistance and inductance of shunt and series filters
C_{dc}, V_{dc}	Dc bus capacitance and voltage
i_{ph}	Photocurrent source
id	Forward diode carrying current
T	Variation in PV cell temperature

Pw	Wind power
PL	Load power
PEV	EV power
$V^{ref}{}_{dc}$	Reference DLCV
Δi_{dc}	Error current
$i_{l\_d} i_{l\_q}$	Load side current in dq component
$V^{ref}{}_{s\_d} V^{ref}{}_{s\_q}$	Reference supply current in dq component
$V^{ref}{}_{l\_abc}$	Reference load terminal voltage in abc phase
$V_{s\_d} V_{s\_q}$	Source voltage in dq frame

1 Introduction

In recent decades, there has been increased focus on incorporating renewable energy sources (RES) into the distribution network. This integration is encouraged to alleviate the workload of VSCs and minimize the need for higher ratings. A novel configuration of a solar-integrated UPQC was created to efficiently tackle PQ issues. The study thoroughly summarizes the difficulties renewable energy sources (RESs) offer and the several approaches taken to overcome these difficulties [1–3]. Because of the inherent uncertainty of PV systems, the electrical grid might experience distortions that affect both voltage and current signals. Custom devices have been utilized to mitigate THD and address voltage stability concerns. Because of the inherent uncertainty of PV systems, the electrical grid might experience distortions that affect both voltage and current signals. FACTS technologies are frequently used to improve PQ. By integrating FACTS, stability in voltage problems is successfully resolved while enhancing the grid's overall PQ [4–6].

An investigation was conducted to see if the use of UPQC in grid-connected solar systems can improve PQ [7]. An exhaustive examination was performed on the characteristics, methods of charging, and advantages of electric vehicles (EVs) [8–10]. The UPQC outperforms the static compensator and DVR in terms of its multifunctional abilities in FACTS. The majority of the intended goals—including raising power factor (PF), diminishing THD, boosting voltage profiles, and generally boosting PQ throughout the system—are successfully attained by the UPQC [11]. The FLC was used to integrate BESS and EVs to provide better power quality, which increased the overall reliability of the grid-associated SPV-WES-BESS-EVs system compared to a conventional grid setup [12].

The firefly optimization method mimics the interaction between predators and prey and was used to obtain optimal parameters of the shunt filter along with PI controller gain values to decrease THD and improve PF [13]. The PI controller gain values selection for the shunt filter was developed utilizing an Ant Colony Algorithm to minimize THD with different loads [14]. An innovative method that combines FLC and NNC was presented to optimize THD and improve PF of five-level UPQC [15]. However, in the distribution network that is linked with a micro-grid, problems over PQ were addressed by introducing UPQC, which aims to address voltage imbalances and current harmonics. Besides, an AI-based ANFIS controller was suggested to improve system efficiency and utilization [16]. A novel control technique, integrating Bat and Mothflame Algorithms, was developed to address PQ issues in a distribution system. The primary objective of this technique is to reduce the error associated with supply voltage fluctuations. In addition, by adjusting the gain parameters, the operational expenses of non-conventional sources decreased [17].

Additionally, a new method that combines Enhanced Efficient Global Optimization with Artificial Neural Network approaches was proposed for SHAPF. The purpose of this method was to reduce existing disturbances and improve the PQ in the distribution system [18]. Furthermore, a study

was undertaken to analyze the power flow of the UPQC by considering an approach of impedance matching under various operating situations [19]. A self-tuning filter technique was developed for UPQC and renewable energy to address PQ challenges [20]. Simultaneously, an ANN was used to apply the PV integrated UPQC to reduce the THD of the grid current and sag and swell in voltage under various load conditions [21]. A novel metaheuristic algorithm named Fennec Fox Optimization (FFA) was developed, which emulates two inherent characteristics exhibited by the Fennec Fox in its native habitat. Fennec's tunneling prowess and ability to evade wild predators served as the primary source of inspiration for the projected FFA [22]. The micro-grid was introduced, which is associated with a direct current (DC) bus that serves as a connection point for various loads. Additionally, the integration of UPQC was employed to address PQ issues [23]. A novel control approach based on synchronous reference frame (SRF) was introduced to address PQ issues. The system utilizes a three-phase four-wire UPQC to mitigate the effects of imbalanced and distorted load situations [24]. A hybrid controller was developed with a soccer league algorithm and is trained using an ANNC to control the shunt active power filter of UPQC. Additionally, this study introduces an FLC in the series active power filter to mitigate the unbalanced supply voltages [25]. The various AI-based techniques with metaheuristic optimization methods were adopted to handle PQ issues and effective management [26–30].

Most existing works focus on UPQC either as a power quality device only, where conventional controllers (e.g., PI, PID) are used for harmonic compensation, voltage sag mitigation, or reactive power control, with limited adaptability to nonlinear or fluctuating loads or an energy management component, where intelligent controllers like FLC or machine learning are applied in smart grid scenarios, but without optimizing UPQC parameters or addressing real-time power quality issues under renewable and EV load integration. Our approach combines both dimensions, i.e., FFOA is used to finely tune NNC, filter parameters of UPQC converters, enhancing response speed, DC bus voltage stability, and efficiency under variable load and fault conditions. Next, FLC handles real-time decision-making for power flow, EV charge/discharge/prioritizing source allocation (e.g., between renewables and grid), and ensuring power quality compliance even during unpredictable load/generation fluctuations. This hybrid structure allows the UPQC to act not only as a power quality solution but also as an active participant in energy optimization, particularly in microgrids or smart distribution systems with high renewable penetration. It is essential to mention that, especially when there is high demand for electricity on the grid, both BESS and EVs can effectively control and handle excessive power demand. This dual strategy enhances PQ and enables simultaneous power flow regulation. The novelty of the paper is highlighted in the key points below:

- Application of the FLC to handle the power flow among the RES, WES, Grid, and EVs.
- Training of NNC for shunt inverter along with the choice of filter parameter values of five-level cascaded H-Bridge UPQC by using FFOA to reduce mean square error (MSE) and THD.
- Reduction of THD in the current improves PF, and addresses issues with grid voltage such as disturbances, swells, sags, and other associated difficulties.
- The integration of EVs, BESS, and RES to UPQC helps to minimize the stress on converters, and offers support in satisfying the demand, and guarantees the regulation of a stable voltage across the DC bus, even in the presence of fluctuations in solar radiation (G), wind speed, and load.

The paper is organized in the following manner: Section 2 gives the modeling of renewable sources, Section 3 focuses on applying the approaches employed in this research, specifically Fuzzy and FFOA. Section 4 provides the findings and corresponding analysis. In conclusion, Section 5 provides

a comprehensive overview of the findings derived from the proposed study and proposes prospective avenues for further research within this particular domain.

2 Modeling of Microgrid

Here, two inverters coupled to a single DC-link capacitor buildup the UPQC. The shunt converter is attached in parallel to the point of common coupling (PCC), and the series converter is connected through a series transformer. Whereas the shunt converter functions as a current source, the series converter serves as a voltage source. Fig. 1 shows the schematic layout of the proposed system. The WES, SPV, BESS, and EV grid connections enable PQ control and parallel power management. The primary function of the series filter is to address grid-side voltage-related issues. This is achieved by providing the right choice of L_{se} and the required V_{se}, delivered the interface transformer. Similarly, the shunt filter is connected to the grid L_{sh}. The shunt filter is responsible for maintaining a constant DLCV and adding compensating currents to suppress the harmonic content in the current.

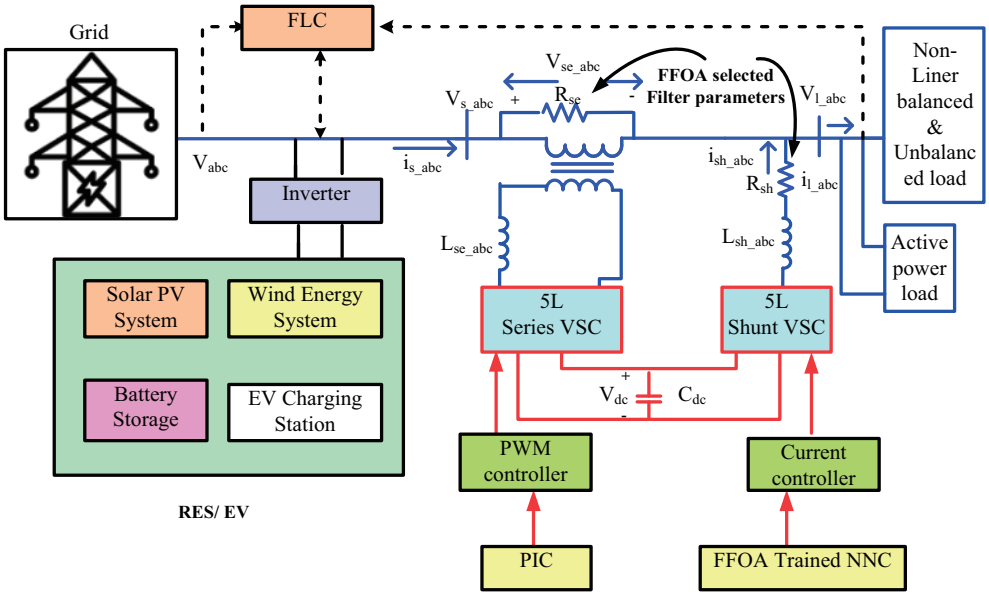

Figure 1: Layout of developed U-SWBEV with FFFO optimized and loads considered

Nevertheless, the primary limitation of traditional converters is that their output contains a significant amount of harmonics, resulting in the need for larger filters to achieve a sinusoidal waveform, which incurs higher costs. In addition, the proposed multilevel converters generate a levelled output, reducing both the size and cost of the converters. In multilayer inverters, the cascaded H Bridge architecture operates without the need for clamping diodes or components. Fig. 2 illustrates the three-phase 5L-CHBU (cascaded H-bridge UPQC) configuration of a one-sided converter, while the corresponding switching sequence is presented in Table 1. The five-level cascaded H-bridge (CHB) topology was chosen over neutral point clamped (NPC) and fuzzy logic controller (FLC) because it 25%–30% lower switching losses with 50% lower THD and simpler and more robust DC link balancing. These advantages directly enhance the performance, reliability, and efficiency of the UPQC, especially in high-power or modular applications. Eq. (1) is used to calculate the power flow.

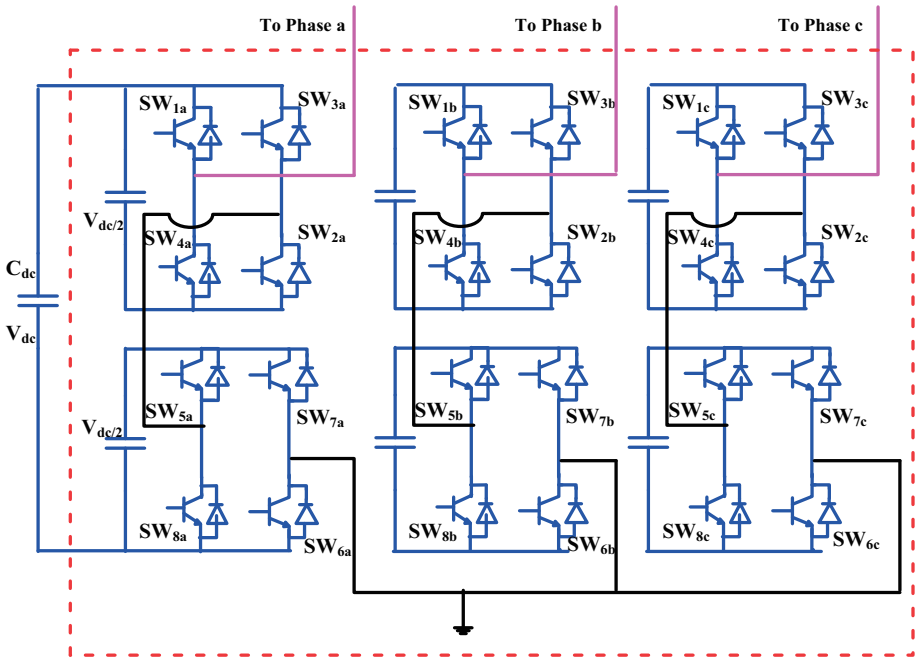

Figure 2: Three phase 5L cascaded H bridge VSC configuration for the proposed UPQC

Table 1: Switching pattern for cascaded five level UPQC

Output	SW-1	SW-2	SW-3	SW-4	SW-5	SW-6	SW-7	SW-8
V_{dc}	✓	✓	*	*	✓	✓	*	*
$V_{dc/2}$	✓	✓	*	*	✓	*	✓	*
0	✓	*	✓	*	✓	*	✓	*
$-V_{dc/2}$	*	*	✓	✓	✓	*	✓	*
V_{dc}	*	*	✓	✓	*	*	✓	✓

Note: ✓ indicates ON, * indicates OFF.

2.1 Modeling of Solar PV System

A solar photovoltaic system operates based on the premise that solar cells convert light energy into electrical energy. The modules of PV are arranged in a series configuration to create a string, which is then assembled in parallel to achieve the desired current and voltage levels.

$$P_{PV} \pm P_{BESS} + P_{w} \pm P_{EV} \pm P_{Grid} = P_{L} \tag{1}$$

Fig. 3 depicts the representation of the single diode model. The system comprises a photocurrent, denoted as I_{ph}, contingent upon temperature and irradiation. The series resistance signifies the internal resistance through which current I is transmitted, while the shunt resistance characterizes $i_{sh,PV}$ flow, representing a leakage current. The equations for the load current, photocurrent, and other variables [24] are provided in Eqs. (2)–(6).

$$I = I_{ph} - I_{0} - I_{sh} \tag{2}$$

$$I_{ph} = [I_{sc} + k_i (T_k - T)] \times \frac{G}{1000} \tag{3}$$

$$I_{RS} = \frac{I_{SC}}{[\exp (q \times V_{oc}/N_s \times k \times A \times T) - 1]} \tag{4}$$

$$I_0 = I_{RS} \left[\frac{T}{T_r}\right]^3 \exp\left[\frac{q \times E_{g0}}{Ak} \left\{\frac{1}{T_r} - \frac{1}{T}\right\}\right] \tag{5}$$

$$I_{PV} = N_P \times I_{ph} - N_P \times I_0 \left[\exp\left\{\frac{q \times V_{PV} + I_{PV} R_{se}}{N_s \times AkT}\right\} - 1\right] \tag{6}$$

here, I_{PV} represents diode photocurrent, V_{PV} denotes diode voltage, I_0 gives reverse saturation current, V_{oc} resembles open circuit voltage, I_{sh} is leakage current, R_{se} denotes series resistance, I_{sc} represents short circuit current, R_{sh} denotes shunt resistance, q represents electron charge, A represents diode ideality factor, k defines Boltzmann constant T is the temperature, N_P-N_s gives the number of PV cells connected in parallel/series.

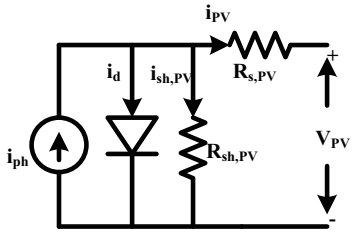

Figure 3: PV single diode cell

2.2 Battery System

The BESS plays a crucial role in ensuring satisfaction of load needs. Batteries, composed of cells assembled in parallel/series configurations, are utilized to get the requisite amounts of voltage and current. The BESS also aids in maintaining DLCV. The Li-ion battery is chosen for this research project because of its benefits, including slow discharging and low maintenance expenses. Eq. (7) represents the SOCOB, whereas Eq. (8) provides the boundaries of this state.

$$SOCOB = 95\left(1 + \int i_{BSS}\, dtQ\right) \tag{7}$$

$$SOCOB_{\min} \leq SOCOB \leq SOCOB_{\max} \tag{8}$$

2.3 Wind Energy System

The wind's kinetic energy is initially transformed into rotational motion, which is then synchronized with the speed of the turbine and generator through a gearbox. A generator's purpose is to transform the mechanical output produced by a turbine into electrical. Through the process of rectifying, the alternating current (AC) voltage produced by WES is converted into a DC voltage. This DC voltage is then increased using a boost converter to enhance its magnitude. This study takes the permanent magnet synchronous machine because it provides reliability, cost-effectiveness, ease of operation, and exceptional performance. The WES controller is depicted in Fig. 4. The Eqs. (9)–(11) provide the power generated by WES [24].

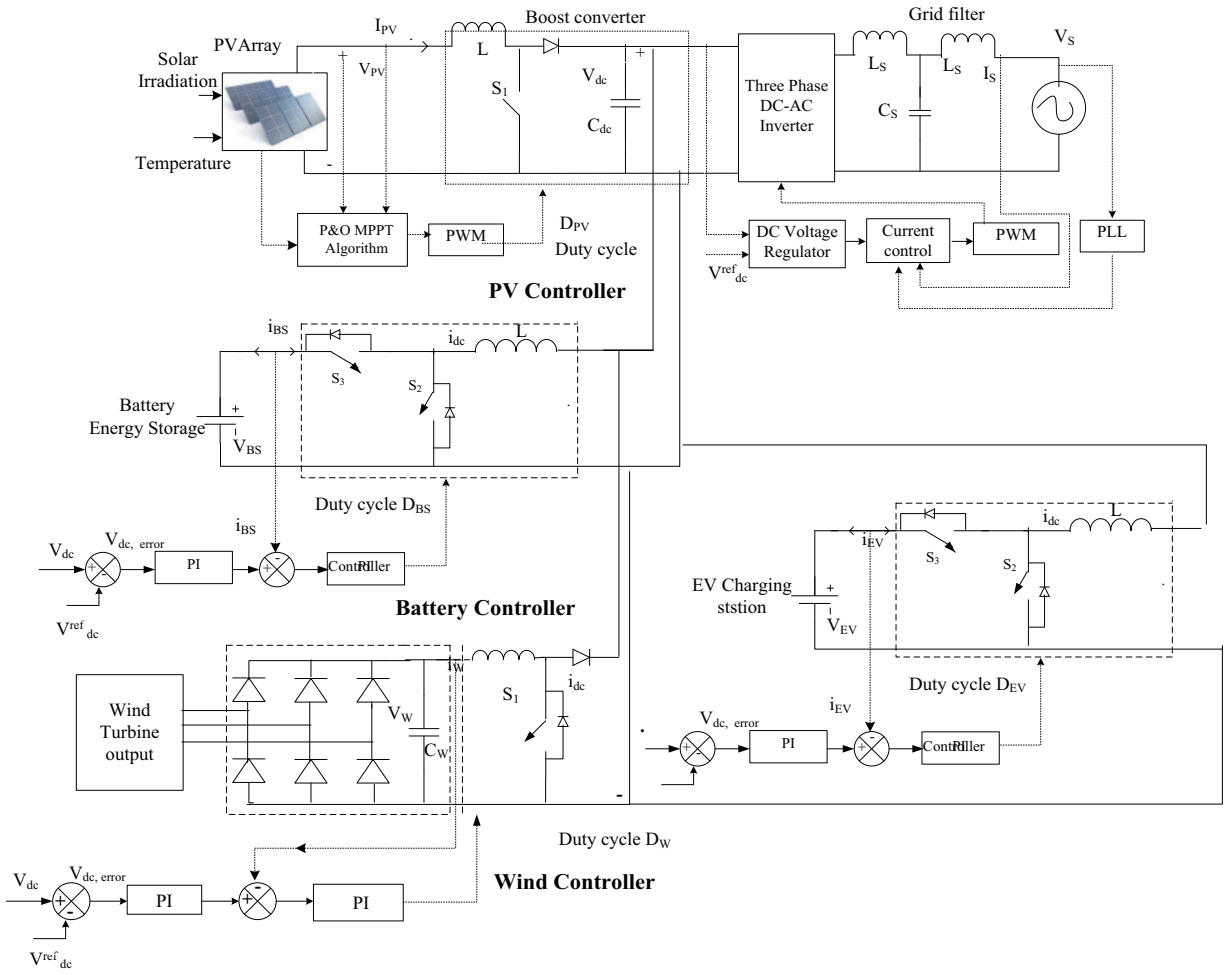

Figure 4: Control of Microgrid/EV charging station at grid side

Here, P_M denotes the mechanical power, β gives pitch angle, ρ represents air density, λ gives the tip-speed ratio, R illustrates blade radius, tip speed ratio $\lambda = \Omega R/V$, Ω denotes rotor speed, and C_P can be expressed as a function of λ

$$P_M = 1/2\Pi\rho C_P(\lambda, \beta) R^2 V^3 \tag{9}$$

$$C_P = 1/2\left(\frac{116}{\lambda_1} - 0.4\beta - 5\right)\exp^{\frac{-165}{\lambda_1}} \tag{10}$$

$$\lambda_1 = \left(\frac{1}{\frac{1}{\lambda + 0.089} - \frac{0.035}{\beta^3 + 1}}\right) \tag{11}$$

where C_P is the power coefficient of the turbine and λ_1 is any constant.

3 Fuzzy Logic-Based Power Flow Control

The utilization of the RES for power production and demand forecasting by the FLC facilitates the management of power shifting between the grid and EVs. It enables the transmission of electrical energy between EVs and the power grid. This study helps in improving PQ and power management in the grid system by integrating EVs with UPQC. The main goal of applying FLC-based power management is to govern the usage of EVs as transportable and BESS. Therefore, once accrued energy is no longer necessary, it can also be used for transport purposes. The triangular MSF is adopted to produce the best result, as illustrated in Fig. 5, and the inputs 1 and 2, output MSF are shown in Fig. 6, respectively. The fuzzy surface area is illustrated in Fig. 7. The mathematical expression for the triangular MSF is presented in Eq. (12).

$$\mu_{Ai}(x), i = 1, 2$$
$$\mu_{Bj}(y), j = 1, 2 \tag{12}$$

where μ_{Ai}, μ_{Bj} are the MSF outputs.

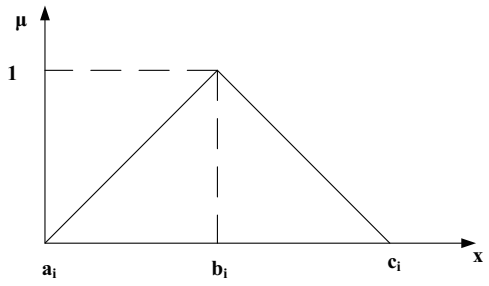

Figure 5: Triangular MSF for FLC

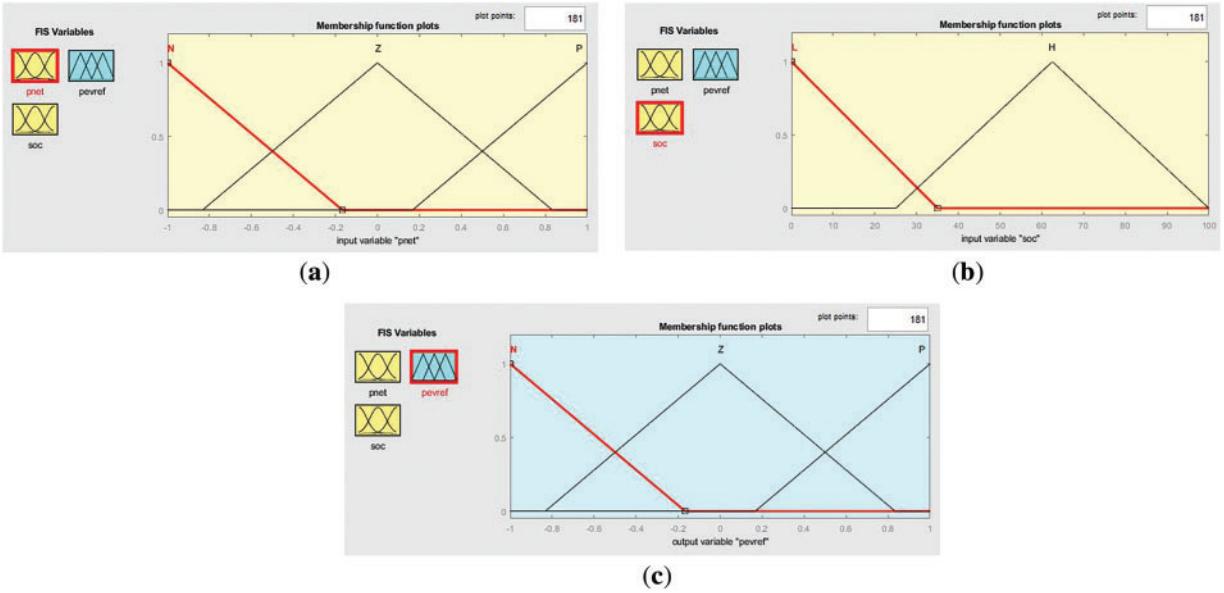

Figure 6: MSF of FLC for power flow control. **(a)** MSF of input-1; **(b)** MSF of input-2; **(c)** MSF of output

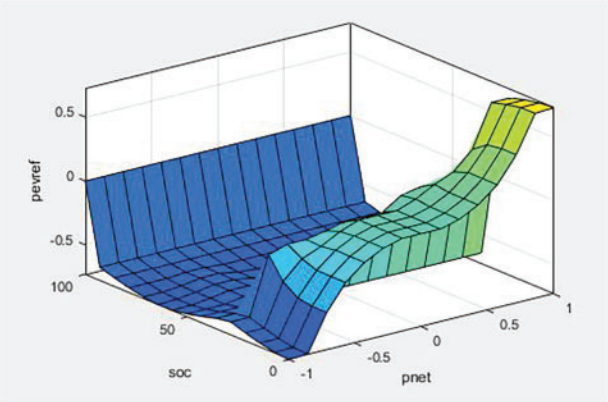

Figure 7: Fuzzy surface

The present study focuses on the efficient management of power flow through the utilization of FLC. The flowchart depicted in Fig. 8 elucidates the operating procedure of the proposed power flow. FLC regulators facilitate power transfer among organizations, such as the grid, BESS, load, and EV charging stations. Nevertheless, this factor is crucial in determining the course of action regarding EV charging. The EVs can be stored at charging stations when not in use. These electric vehicles can also serve as BESS during periods of heavy demand, decreasing the peak load hours of the grid. Essential loads (e.g., healthcare equipment, communication systems) are served with the highest priority to ensure reliability. During peak demand, the BESS discharges to support the grid or local loads, helping reduce peak power drawn from the utility. EV charging is reduced or temporarily deferred if it's not time-sensitive or if the state of charge (SOC) is sufficient for expected travel needs. EVs can discharge stored energy back to the grid during peak times, acting as mobile energy storage. EVs provide backup power to the home or building loads during outages or peak pricing hours. Charging schedules are optimized based on grid demand and user preferences. Charging and discharging are constrained within optimal SOC ranges (typically 20%–95%) to minimize battery stress. The energy management system minimizes unnecessary cycling by aggregating demand and utilizing other energy sources (e.g., solar, wind, grid) when economically or technically viable. Scheduled charging/discharging is considered to avoid overuse. The visual representation of the fuzzy-based power flow control is illustrated in Fig. 9.

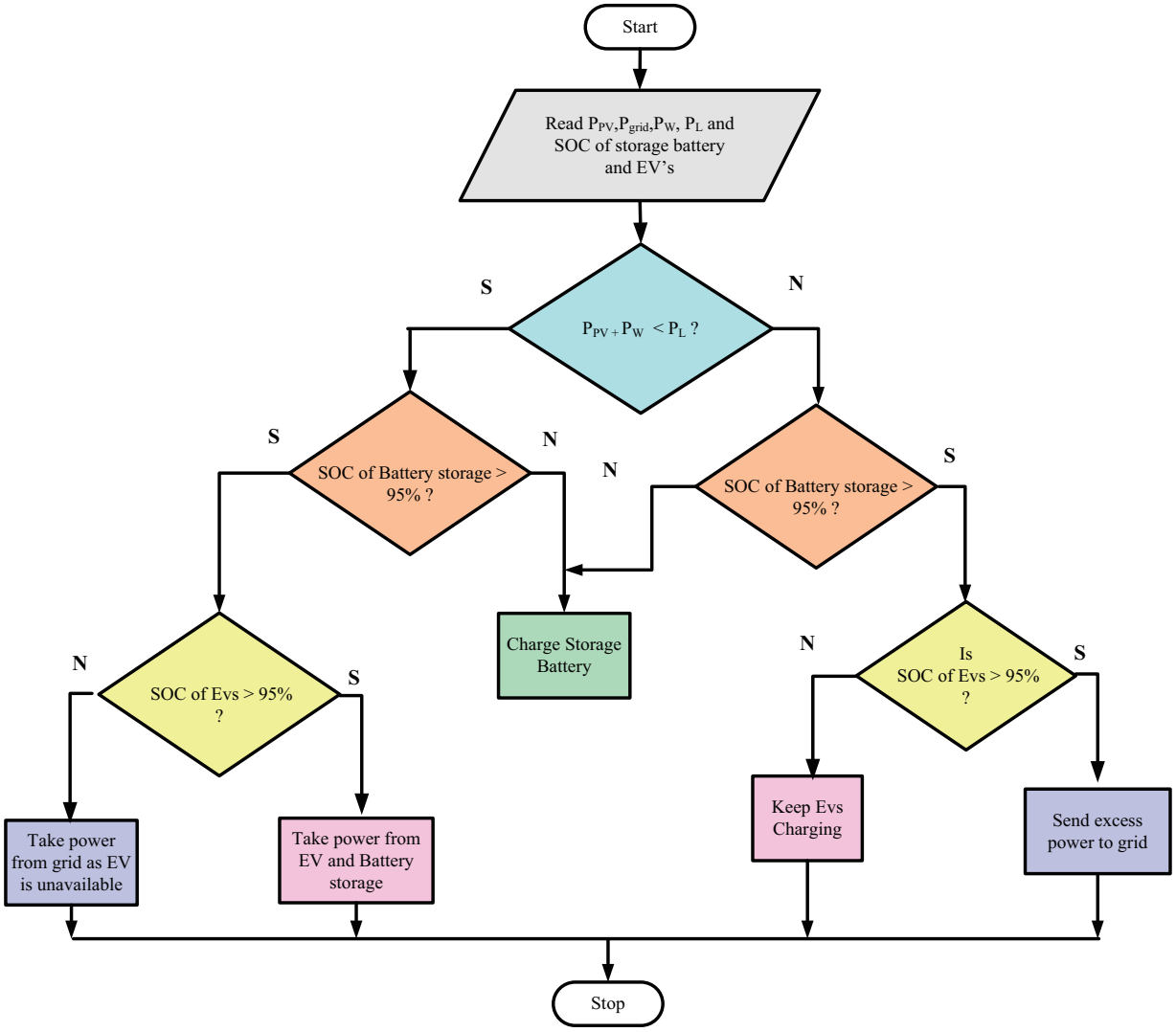

Figure 8: Power flow chart

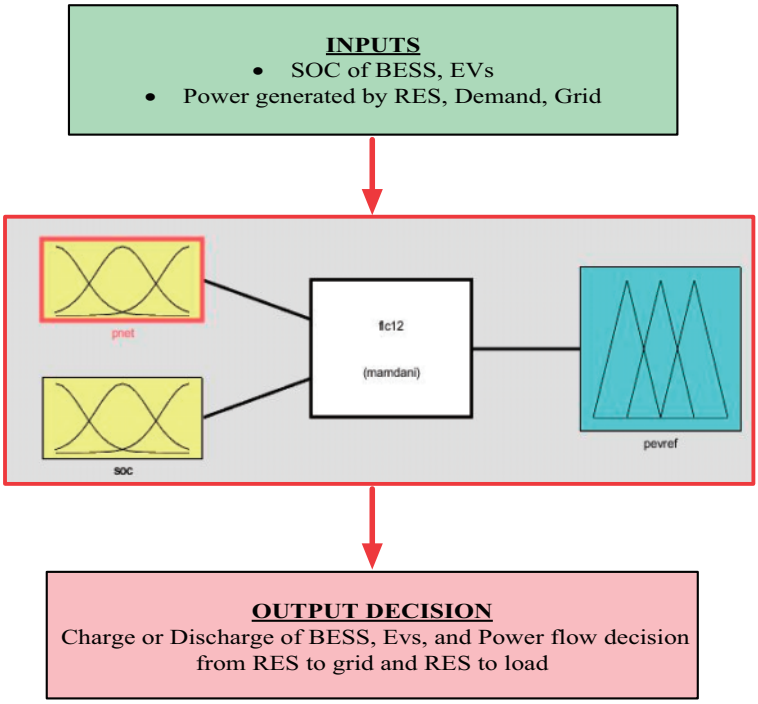

Figure 9: Fuzzy logic-based power flow control

4 Proposed Controllers

The shunt filter reduces THD in the current signal and stabilizes the DC bus voltage. This is achieved by employing the abc/dq0 transformation, utilizing the optimally trained NNC with FFOA, and carefully selecting filter settings. However, to convert sources into a dq0 frame, the PLL utilizes phase and frequency information obtained from the supply voltage. The FFOA-NNC compares the V_{dc} and $V^{ref}{}_{dc}$ to maintain it stable. It then makes appropriate current changes to rectify any differences. The load current's d-th component is incorporated into the NNC. The Hysteresis controller depicted in Fig. 10 is utilized to create gate signals. ANN is a renowned technique in the field of Artificial Intelligence. It is a mathematical model inspired by humans and is highly versatile for controlling electrical systems. Multi-layer perceptrons (MLPs) encompass the well-known neural networks. The benefits of ANN include its capacity for self-learning, fault tolerance, rapid convergence, and robustness. The layout of an ANN has 3 layers: (IL, HL, OL), input/hidden and output layers. The learning algorithm chosen for training is the primary determinant of ANN performance. Training is the iterative process of identifying the optimal set of weights that connect the neurons of the NN across different layers to minimize errors. There are primarily two types of training methods in MLP: supervised and unsupervised.

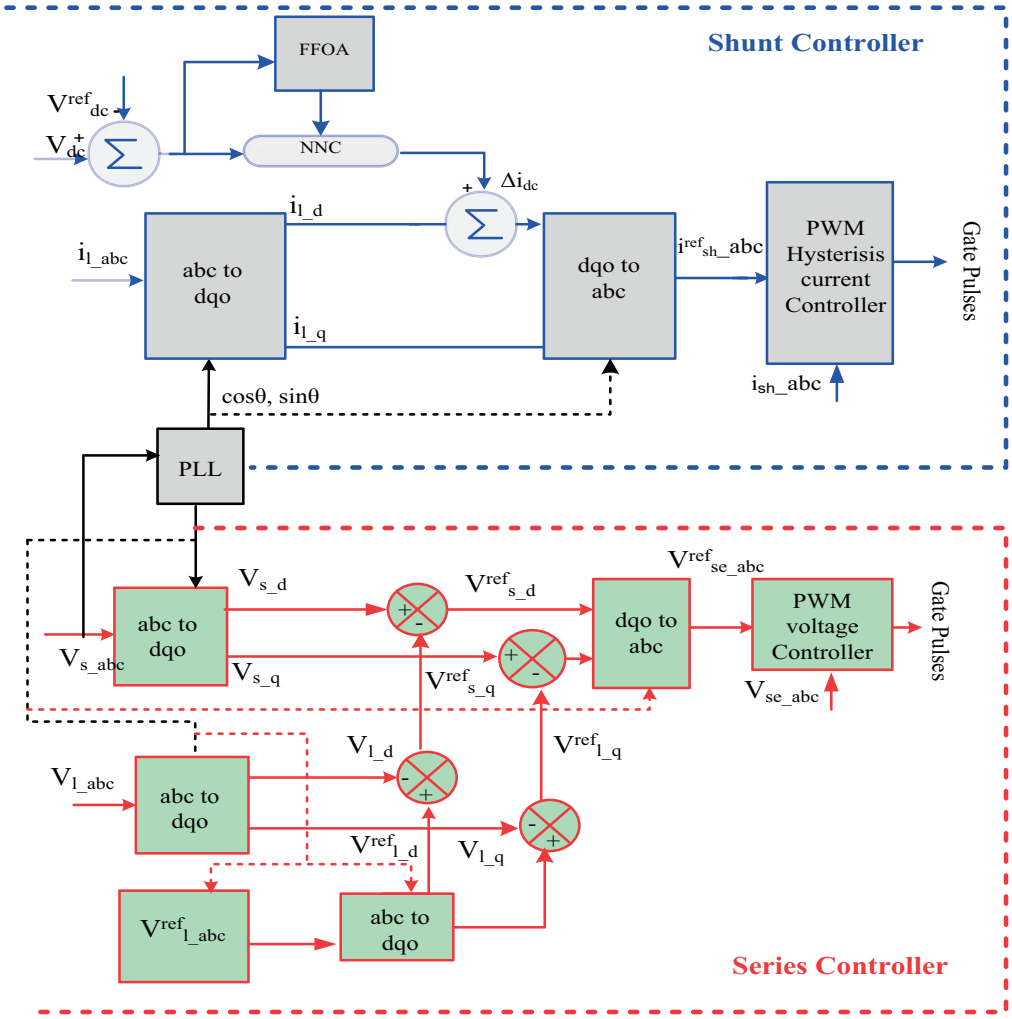

Figure 10: Control of shunt and series converters of UPQC

However, these methods can be classified into gradient search and meta-heuristic. Back propagation (BP) is a well-known training approach for MLP networks that is based on gradients. Despite its fame, BP is plagued by several shortcomings, including inadequate initial weight estimation, sluggish convergence, and a high likelihood of becoming stranded in local minima. In addition, search methods based on meta-heuristic algorithms rely on the stochastic choice of preliminary predictions at the time of the optimization procedure. Utilizing these methods offers the advantage of identifying the global best optimal solution as opposed to a local optimal solution. Nevertheless, they require any preexisting knowledge of the selected issue during calculation. The approaches above can be utilized to optimize the weight, parameters, and design of neural networks NN. In supervised learning, the objective is to reduce the disparity between the intended and output. The summation function aims to aggregate the product of inputs, weights, and bias, as depicted in Eq. (13). In this equation, wt_{pk} represents the connection weight I_p linking neuron k, β_k represents a bias term, and m is the total number of inputs for the neuron. A nonlinear activation function, such as the sigmoid function, is commonly employed as indicated in Eq. (14). Hence, the output of neuron k can be characterized as depicted in Eq. (15).

$$S_k = \sum_{p=1}^{m} wt_{pk} I_p + \beta_k \tag{13}$$

$$f(x) = \frac{1}{1 + e^{-x}} \tag{14}$$

$$O_k = f_k \left(\sum_{p=1}^{m} wt_{pk} I_p + \beta_k \right) \tag{15}$$

The present study involves training of feed-forward structure with a single-layer NN for DC bus voltage stabilization. The NN is then compared to a reference model, where the error is utilized as the input and the intended output is provided as the target to the NN. Reduced Complexity by using fewer layers or fewer neurons per layer (10 neurons with 1 hidden layer), early stopping the training when the validation loss stops improving, even if training loss continues to decrease, and reducing training time with fewer epochs (1000) to avoid the model memorizing the training data. The structure of NN for the shunt DC-bus voltage balancing with 10 neurons in HL is depicted in Fig. 11, while Fig. 12 illustrates the design of the FFOA trained NNC controller for DC-Link. A study [25] demonstrated that a multilayer perceptron with one hidden layer is sufficient for approximating any type of function.

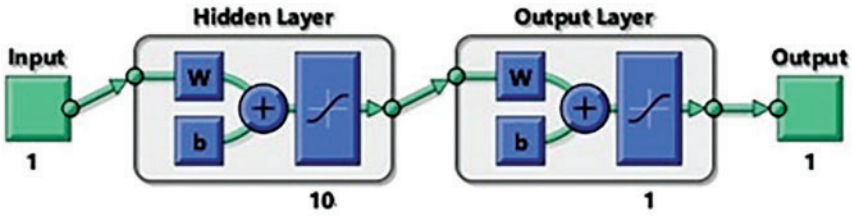

Figure 11: Structure of artificial neural network controller (ANNC) for DC-link with number of neurons and layers

The voltage across the load terminals is compared to a specified reference value using proportional integral controller (PIC) after conversion from the abc-dq0 domain and *vice versa*. This process subsequently generates the fundamental gate pulses for the series filter. The present signals function as the initiating pulses for implementing PWM in the converter.

4.1 FFOA Selection of NNC Bias, Weights, and Parameters

The multilevel UPQC with conventional design parameters may not be effective in lowering the THD. In recent days, meta-heuristic optimization algorithms have played a vital role in solving complex multi-objective engineering problems effectively. In this work, FFOA, a member of the meta-heuristic algorithm family, is employed for solving the UPQC design problem to minimize the THD and obtain the best possible design parameter values for both the series and shunt converters of UPQC, taking into account various power quality problems at different harmonic loads. The main reason for selecting FFOA in this work is its advantages, such as its effectiveness in solving unconstrained and constrained multi-objective optimization problems, easy development, minimum parameters for tuning, and robust solutions. This section explains the FFOA, the representation of problem variables the solution procedure.

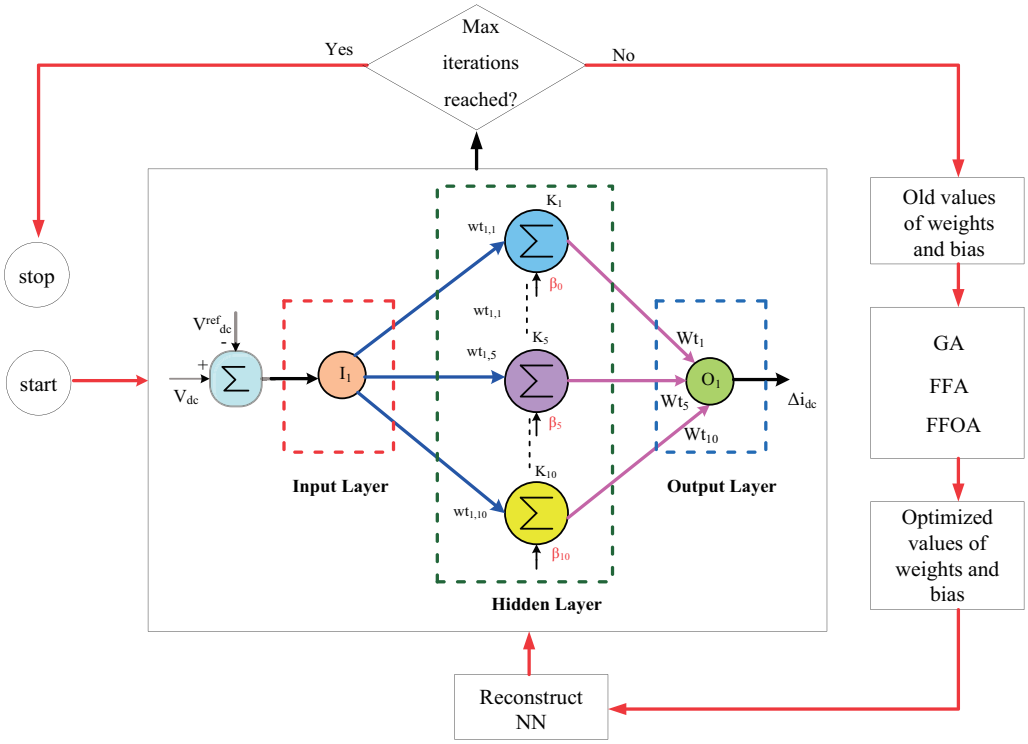

Figure 12: FFOA trained NNC for DC-Link voltage management

The fennec fox is an omnivorous creature that consumes a variety of food sources, such as lizards and small rodents. The significance of the two actions exhibited by the fennec fox surpasses that of its other characteristics. The proposed FFOA optimization method draws inspiration from the main elements of a powerful digging ability and an escape plan from predators. Below, a comprehensive explanation of the mathematical modelling is provided.

4.1.1 Initialization

FFOA utilizes a population of fennec foxes as members in search space. In FFOA, every fox symbolizes a potential resolution to the problem, and its placement inside the search space dictates the value assigned to the decision variables. A fennec fox can be mathematically represented as a vector, while its population can be defined as a matrix known as the population matrix [22]. During the initialization process, foxes are randomly assigned using a value of Eq. (16).

$$X_i: x_{i,j} = lb_j + r.\left(ub_j - lb_j\right), \quad i = 1, 2 \ldots N, j = 1, 2 \ldots m \tag{16}$$

In this context, X_i represents the i-th fox, $x_{i,j}$ denotes the j-th dimension, corresponding to the control parameter. N represents the total foxes, m signifies the total number of control parameters, r is a randomly generated number within the interval [0, 1], lb_j and ub_j represent the lower and upper bounds of the j-th decision variable. The matrix with the population of N fennec foxes for the FFOA is defined in Eq. (17).

$$X = \begin{bmatrix} X_1 \\ . \\ . \\ . \\ X_i \\ . \\ . \\ . \\ X_N \end{bmatrix}_{N\times m} = \begin{bmatrix} x_{1,1} & . & . & . & x_{1,j} & . & . & . & x_{1,m} \\ . & . & & & . & & & . & . \\ . & & . & & . & & . & & . \\ . & & & . & . & . & & & . \\ x_{i,1} & . & . & . & x_{i,j} & . & . & . & x_{i,m} \\ . & & & . & . & . & & & . \\ . & & . & & . & & . & & . \\ . & . & & & . & & & . & . \\ x_{N,1} & . & . & . & x_{N,j} & . & . & . & x_{N,m} \end{bmatrix}_{N\times m} \tag{17}$$

The matrix X denotes the i-th fennec fox within the population, spanning the range provided by N, denoted as $X_i = (x_{i1}, x_{i2}, \ldots, x_{im})$. Each column $x_{1j}, x_{2j}, \ldots, x_{Nj}$ symbolizes the potential value for the j-th decision variable. Each fennec fox proposes possible values that are then assigned to the objective function variables, which are then assessed. The objective function's estimated values are formally represented using the vector stated in Eq. (18).

$$F = \begin{bmatrix} F_1 \\ . \\ . \\ . \\ F_i \\ . \\ . \\ . \\ F_N \end{bmatrix}_{N\times 1} = \begin{bmatrix} F(X_1) \\ . \\ . \\ . \\ F(X_i) \\ . \\ . \\ . \\ F(X_N) \end{bmatrix}_{N\times 1} \tag{18}$$

F represents the vector of objective (obj) function values, while F_i represents the value of the obj calculated for the i-th fennec fox. The position of foxes has been updated using two natural fennec fox behaviors. These activities include (i) excavating to consume prey deep within the sand and (ii) escaping predators.

4.1.2 Stage 1: Digging for Prey (Exploitation)

The fennec fox does nocturnal hunting, utilizing its heightened auditory capabilities to locate prey beneath the sandy surface. Once located, it employs its feet to excavate and pursue its prey. The action exhibited by the fennec fox can be characterized as a local search. By imitating this behavior, the FFOA's ability to utilize the environment is enhanced, leading to a solution that is closer to the global optimal solution. To simulate the actions of a fox while digging, we examine a local area with an R radius surrounding its current location. A fox conducting a local investigation in this location can reach a superior solution. The mathematical simulation of updating members is performed using Eqs. (19)–(21).

$$X^{P1}{}_{i,j} = x_{i,j} + (2.r - 1)\,.R_{i,j} \tag{19}$$

$$R_{i,j} = \alpha.\left(1 - \frac{t}{T}\right).x_{i,j} \tag{20}$$

$$X_i = \begin{cases} X_i^{P1}, & F_i^{P1} \le F_i \\ X_i, & else \end{cases} \tag{21}$$

The new status of i-th fox, denoted as $X^{P1}{}_i$, is determined based on the first phase. The dimension of $X^{P1}{}_{i,j}$ is the j-th dimension, the objective function value is represented by $F^{P1}{}_i$, the neighbor radius for $x_{i,j}$ is known as $R_{i,j}$, the iteration counter is denoted as t, the total iterations is denoted as T, and the constant α is set to 0.

4.1.3 Stage 2: Escaping from Prey (Exploration)

Wild predators threaten the fox, like the Pharaoh eagle-owl, etc. Nevertheless, it evades predators due to its remarkable velocity and abrupt alteration of locomotion. The escape method employed by the fennec fox serves as the foundation for the comprehensive exploration of the search space within a mathematical model. It aids in avoiding being trapped in the most efficient local regions and thereby locating the most efficient global one. Therefore, the stochastic placement of each potential solution inside the search space can represent the fennec fox's behavior [22] while attempting to evade capture. The mathematical simulation of the 2nd phase of population is updated by using Eqs. (22)–(24).

$$X^{rand}{}_i : x^{rand}{}_{i,j} = x_{i,j}, k \in \{1, 2 \ldots N\}, i = 1, 2 \ldots N \tag{22}$$

$$X^{P2}{}_{i,j} = \begin{cases} x_{i,j} + r.\left(x^{rand}{}_{i,j} - I.x_{i,j}\right), F^{rand}{}_i \leq F_i \\ x_{i,j} + r.\left(x_{i,j} - x^{rand}{}_{i,j}\right), else \end{cases} \tag{23}$$

$$X_i = \begin{cases} X^{P2}{}_i, F^{P2}{}_i \leq F_i \\ X_i, else \end{cases} \tag{24}$$

Let $X^{rand}{}_i$ represent the position of the target planned for the escape of i-th fox. $x^{rand}{}_{i,j}$ denotes the j-th dimension of the fox, while F and i represent the objective function value. $X^{P2}{}_i$ represents the updated position of the i-th fox established on the second stage. $X^{P2}{}_{i,j}$ represents the j-th dimension of the fox, and $F^{P2}{}_i$ represents the obj value. I is a randomly selected value from the set {1, 2}.

4.1.4 Representation of Design Variables

The problem variables in this study encompass the design parameters, such as the weights and bias of the NNC, as well as the resistance and inductances of both series and shunt active filters. The FF is represented by arranging these variables in vector form, as illustrated in Eq. (25).

$$X = [wt_{1,1} \ldots wt_{1,5}, \ldots wt_{1,10}, \beta_0, \ldots \beta_5, \ldots \beta_{10}, R_{sh}, R_{se}, L_{sh}, L_{se}] \tag{25}$$

where, n = number of design variables

4.1.5 Fitness Function

The objective function used for this study is the minimization of THD. The fitness function (FF) is considered to be the inverse of the objective function, as expressed in Eq. (26).

$$MaxFF = \frac{1}{1 + \{Obj_1, Obj_2\}} \tag{26}$$

where, the Obj_1 = THD determined by Eq. (27).

$$THD = \frac{\sqrt{(I^2{}_2 + I^2{}_3 + \ldots I^2{}_n)}}{I_1} \tag{27}$$

Objective two is denoted as Obj_2, $Obj_2 = MSE$ can be assessed using Eq. (28). In this equation, the actual output is represented, the expected output is indicated.

$$MSE = \frac{1}{n}\sum_{p=1}^{m}\left(O_p - \overline{O}_p\right)^2 \tag{28}$$

4.1.6 Solution Process of the Flow Chart

The FFOA iteration is finished once the position of all foxes is determined in the two phases. The updating procedure persists until the algorithm reaches the maximum number of iterations, as indicated by Eqs. (18)–(23). Ultimately, the FFOA offers the potential resolution to the provided issue following complete execution. The flowchart in Fig. 13 illustrates the stages involved in implementing the FFOA. The bonds of the variables considered in this work were listed in Table 2. On the other hand, FFOA's performance may degrade with the increasing dimensionality of the problem, which is common in large grid power systems. Computational complexity can lead to longer processing times as the size of the grid and the number of variables increase. While FFOA can effectively avoid local optima, its convergence rate may be slower compared to other optimization algorithms, especially in high-dimensional search spaces. In large grid applications, finding the right set of parameters becomes more complex and time-consuming. However, in large power grids, obtaining comprehensive and high-quality data for all components can be challenging, potentially affecting the algorithm's performance.

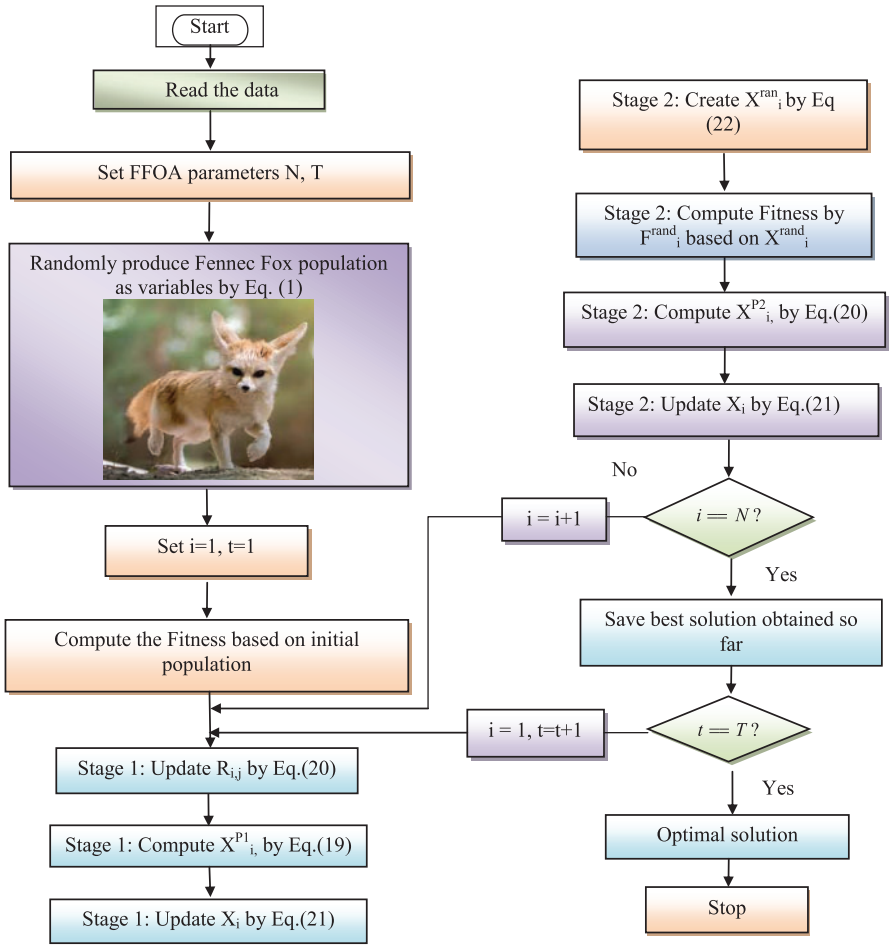

Figure 13: FFOA flow chart

Table 2: Lower and upper bonds for filter decision variables

Decision variable	R_{se}	R_{sh}	L_{se}	L_{sh}
Lower	0	0	0.01	0.01
Upper	10	0.5	10	10

5 Results and Discussion

The development and implementation of the 5LU-SWBEV integrated with FLC were carried out utilizing Simulink/Matlab 2022b. Table 3 contains the selected parameters for SPV, WES, BESS, and EVs. Table 4 presents the selected system and the chosen parameters for the UPQC and the loads. Renewable penetration level can be considered up to 60% of the total load, EV integration is up to 35% of total demand, including clustered charging scenarios. Beyond these thresholds, the THD began approaching the upper limit (5%), and voltage deviations at the PCC exceeded ±5% under worst-case loading, indicating a need for support of energy storage. This research comprises three case studies examining different permutations of voltage issues, including swell, disturbance, and sag. These cases (listed in Table 5) also consider scenarios involving varying irradiation and the velocity of wind. These case studies showcase the efficiency of the created FLC in power management and the integration of FFOA-trained NNC with 5LU-SWBEV. The major aim of this study centers on the intelligent management of power flow, specifically targeting the efficient resolution of PQ concerns. This goal is accomplished by employing the fuzzy-based power flow management and FFOA optimized UPQC to improve PQ.

Table 3: PV, BESS, EV, wind ratings considered for research work

Equipment	Parameter	Chosen value
PV panel	Parallel and series no of cells	45, 10
	SOC	8.18 A
	Rated power	228.735 W
	OCV	37.1 V
	Under $P_{max,}V_{PV}$ & I_{PV}	29.9 V/7.65 A
Li-ion battery	Voltage under fully charged conditions	326.6 V
	Capacity	400 Ah
	SOCB	95%
Wind turbine	Nominal turbine Pmop	30 kW
	Maximum θp	45 deg.
	Base VW	15 m/s
	Maximum rate of change of θp	25 deg./s

Table 4: Grid specifications and Load values selected for the study

Source grid	Voltage: 415 V; Frquency: 50 Hz
DC link capacitor	DC bus voltage: 470 V; DC bus capacitance: 100 μF
Loads selected	1. Rectifier bridge load R = 30; L = 20e−3 2. Active and reactive power load P = 4 kW; Q = 1000 Vars 3. Unbalanced RL load R_1, R_2, R_3 = 10, 40, and 70; L_1, L_2, L_3 = 0.05e−3, 0.1e−3, and 0.15e−3 4. BLDC Motor drive

Table 5: Test Cases considered in the study

Scenario	Case study 1	Case study 2	Case study 3
11 m/s wind velocity	✓	✓	
Stable G	✓		
Varying G		✓	✓
13 m/s wind velocity			✓
Harmonics		✓	
Swell/Sag	✓		
Flicker			✓
Load 1	✓	✓	
Load 2	✓		
Load 3			✓
Load 4		✓	✓
Power factor	✓	✓	✓
THD	✓	✓	✓

Fig. 14a for case 1 demonstrates that the proposed FLC effectively manages EVs in alignment with their SOCs. Currently, the grid consumes power at a rate of 0.1 s, whereas the solar and wind systems generate their power. However, here the BESS will charge, and the EVs will discharge (the vehicle power is sent to the grid) to meet the demand. Next, the grid supplies power at 0.4 s during the charging of EVs, BESS, and PV and wind energy, supplying to their level of extent. In this scenario, (grid to the vehicle) condition exists. At 0.3 s, the grid to island transition takes place where grid power is nil with charging battery and EV, here the required load power is supplied by the islanded renewable source. Besides, Fig. 14b displays the stable G and P_{PV} of the solar system, which has a battery SOC of 95% while exhibiting superior performance in maintaining the stable DLCV.

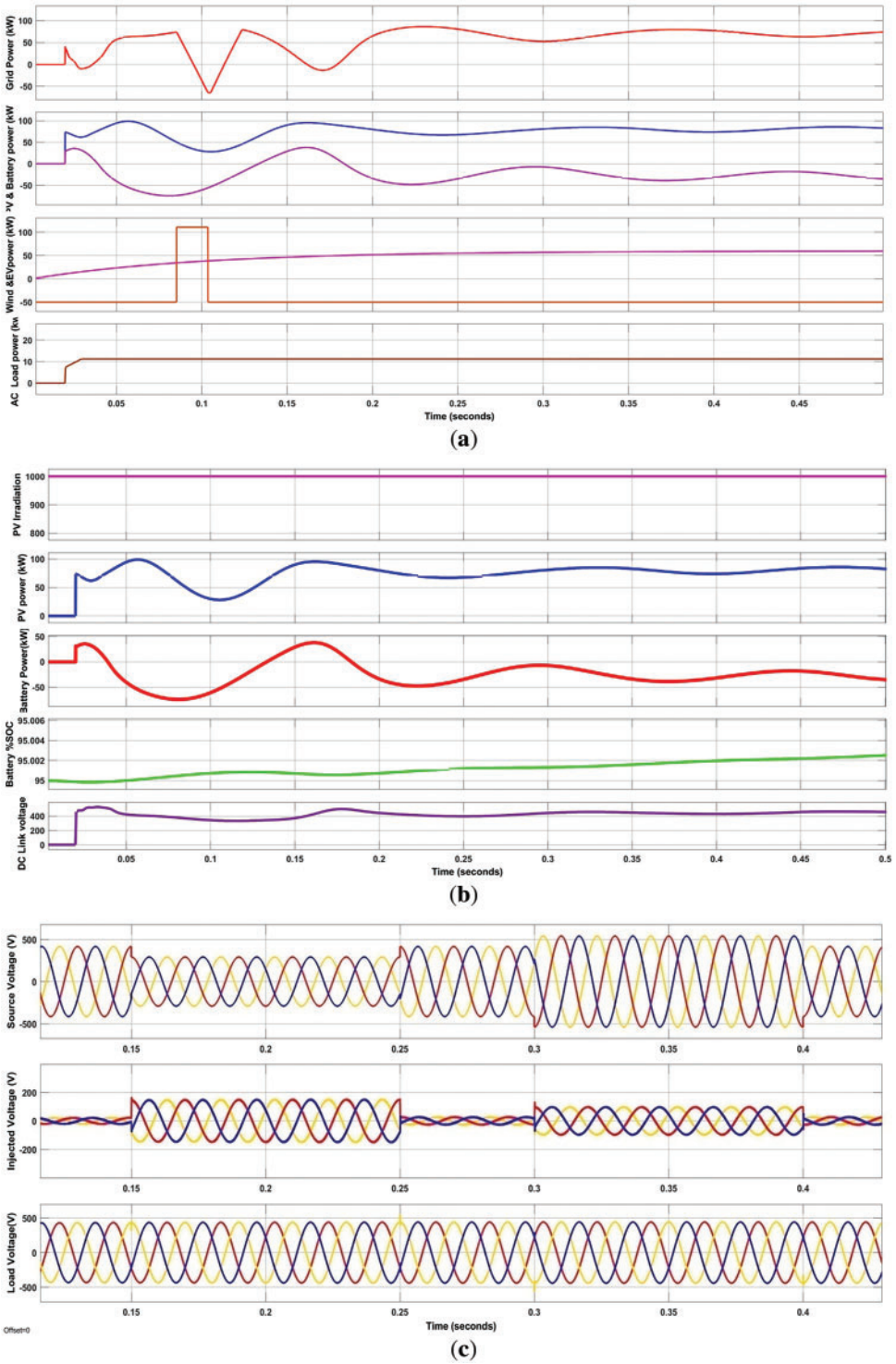

Figure 14: (Continued)

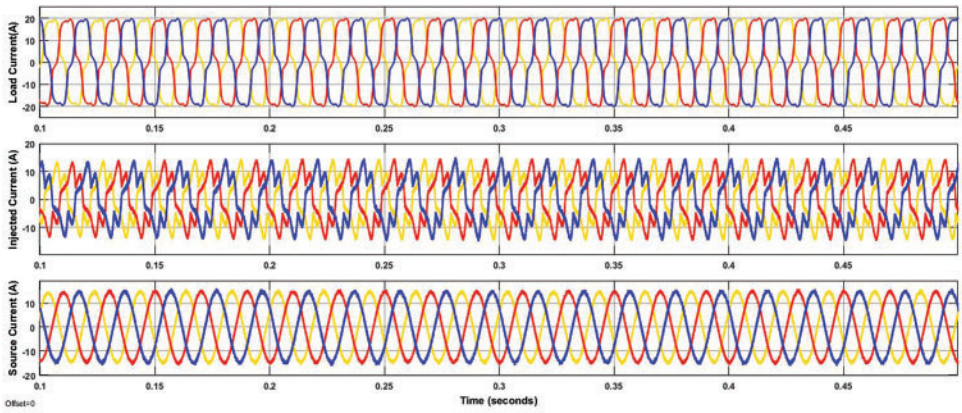

(d)

Figure 14: Waveforms of the FFOA for case 1. **(a)** Powers of grid, solar, battery, wind, EV, load; **(b)** Irradiation, solar battery powers, SOC in %, DC voltage; **(c)** Grid voltage, series filter compensated voltage, load voltage; **(d)** Current at load, compensated current, source current

Fig. 14c illustrates the efficiency of the U-SWBEV in mitigating sag (0.15 to 0.25 s) and swell (0.3 to 0.4 s) through the injection of appropriate voltage for maintaining a steady terminal voltage. In addition, due to the loads 1 and 2, which lead to major distortions of the load current, the SHAPF system ensures the distortion-free grid current by supporting the required amount of compensating current, as depicted in Fig. 14d. This, in turn, minimizes the THD to 2.23% and improves the PF to nearly unity.

In the second case study, it is observed that the proposed approach works effectively during fluctuations in solar G and selected different combinations of loads. In this scenario, the grid consumes power at 0.1 s, as depicted in Fig. 15a, while the RES provides its peak power output. However, EVs are configured to discharge while BESS is in the charging state to provide the required amount of power to the load. On the other hand, the PV and BESS provide nil output at 0.25 s when the EVs are in charging mode. The power is supplied through a combination of a wind system and the grid to satisfy the power requirement. Fig. 15b illustrates the variable G considered during the load transition.

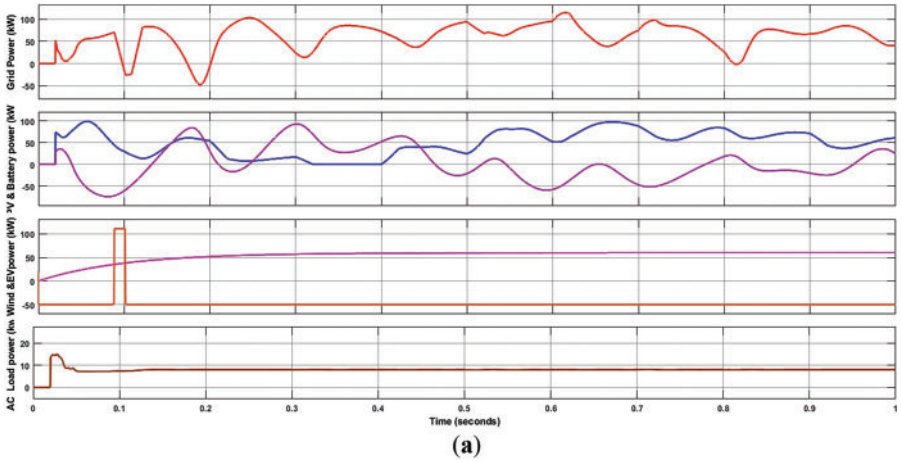

(a)

Figure 15: (Continued)

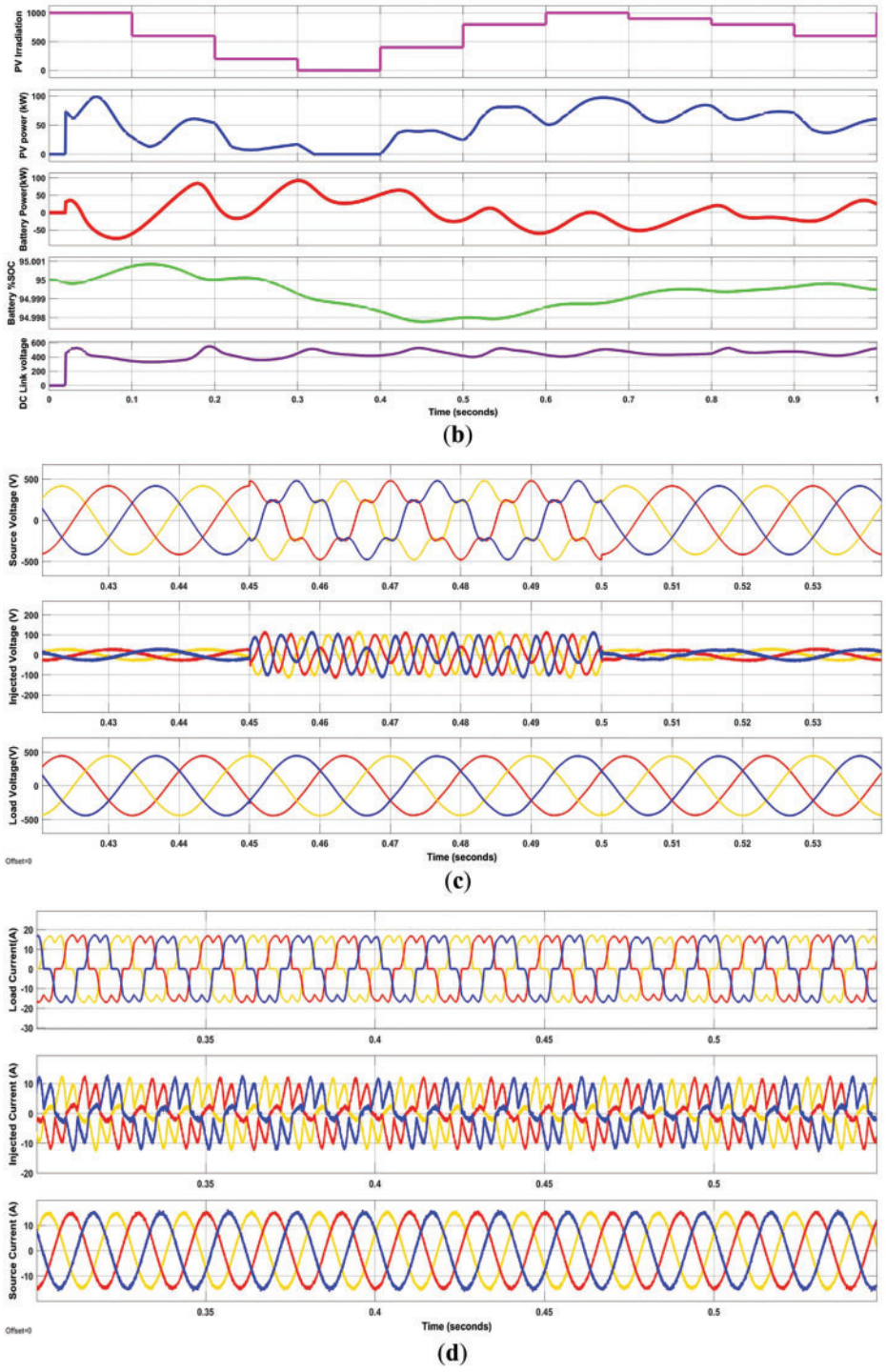

Figure 15: Waveforms of the FFOA for case 2. **(a)** Power of grid, solar, battery, wind, EV, load; **(b)** Irradiation, solar, battery powers, SOC in %, DC voltage; **(c)** Grid voltage, Series filter compensated voltage, load voltage; **(d)** Current at load, compensated current, source current

Furthermore, as highlighted in Fig. 15c, the series filter notably mitigates disturbances occurred during 0.45 to 0.5 s. This is achieved by injecting an appropriate compensatory voltage while maintaining a constant terminal voltage. In addition, due to the nonlinearity of load 1 and load 4, the current at the load terminals is highly polluted. To address this issue, a shunt filter is employed to introduce the required current, as depicted in Fig. 15d, resulting in a reduction of THD to 3.64% and PF close to unity.

In the case 3 scenario, a varying solar G level and load are selected. Specifically, load 3 and load 4 are taken into consideration. The efficiency of the suggested approach is seen in Fig. 16a. The EV provides power to the grid at a time interval of 0.1 s. Besides, it is evident that the grid offers a limited power supply at 0.3 s. Currently, the PV system is insignificant, but the BESS and wind power provide the necessary electricity to the load, while the EV charges from the grid. The selected G, solar power generated, and DLCV balancing with SOC of the battery storage are depicted in Fig. 16b. This study investigates the occurrence of voltage flicker within the time range of 0.2 to 0.3 s, demonstrating the effective mitigation of this issue using the UPQC. In addition, the U-SWBEV efficiently manages the imbalanced load and delivers sinusoidal source current with reduced THD, as depicted in Fig. 16c,d.

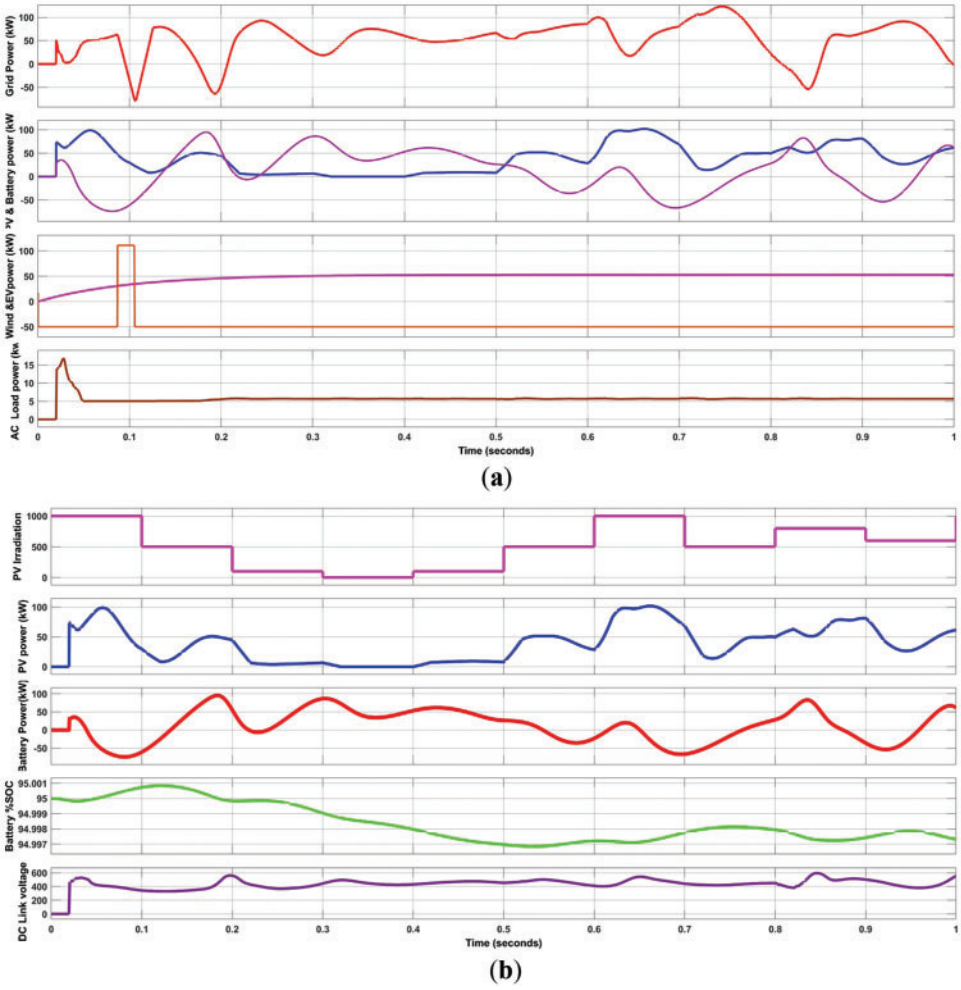

Figure 16: (Continued)

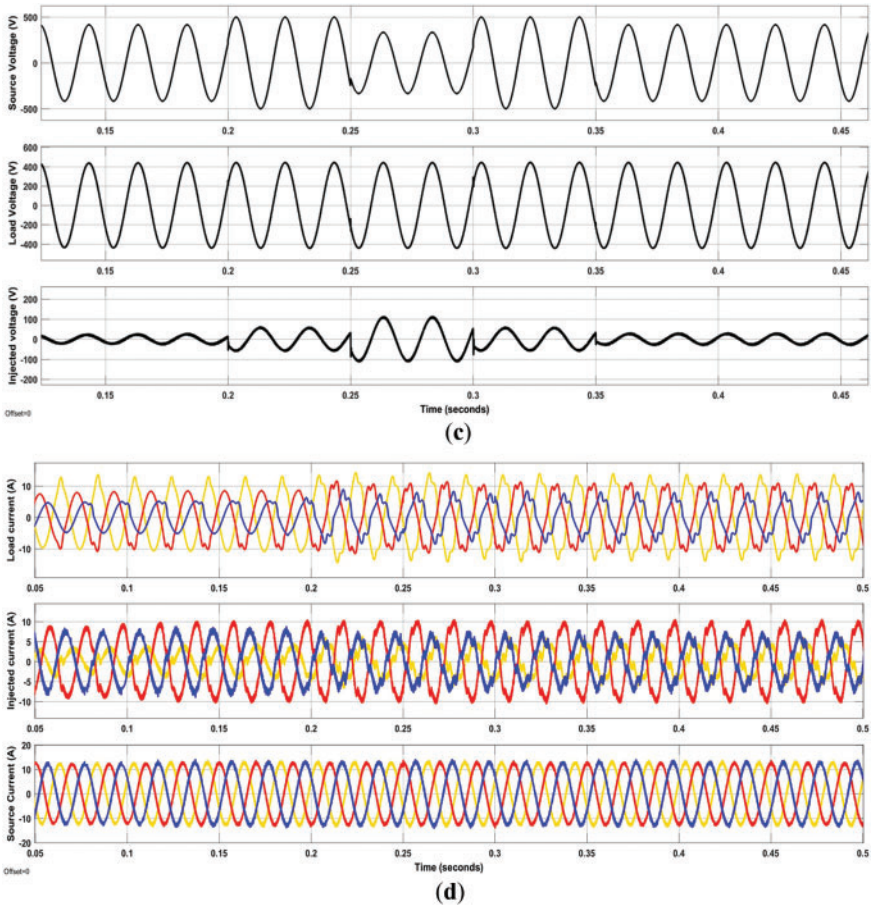

Figure 16: Waveforms of the FFOA for case 3. **(a)** Powers of grid, solar, battery, wind, EV, load; **(b)** Irradiation, solar, battery powers, SOC in %, DC voltage; **(c)** Grid voltage, series filter compensated voltage, load voltage; **(d)** Current at load, compensated current, source current

Table 6 shows the THDs of the suggested technique in each case study. Well, it is exhibited from the outcomes that the obtained THD values in all case studies are within the IEEE 519-2014 standards in addition to the THD when compared with other standard methods, including those found in the review. Below 20%–30% of full load, harmonic-producing rectifiers can dominate current flow, at which THD compliance fails. Additionally, as Fig. 17 illustrates, it has been proven that the suggested FFOA for the five-level converter system converges to a lower THD of 2.23% after 20 iterations. Comparatively, to reach convergence, GA and FFA need 63 and 43 iterations, respectively. Furthermore, as Fig. 18 illustrates, the value of the proposed PF system is extremely close to unity when compared to alternative methods.

Besides, it is clearly visible from Fig. 19 that the time taken (sec) for the proposed method to reach a stable DC bus voltage is much less than other compared techniques. Similarly, Fig. 20 exhibits that the MSE for the suggested approach is lower when compared to other algorithms. In addition, Table 7 included the UPQC optimized parameter values that were acquired. In Fig. 21, the regression curve for NN is displayed. The fast Fourier transformation (FFT) spectrum of the grid current for the suggested system's case studies is shown in Fig. 22. Finally, the statistical comparison of THD

result for case-1 with maximum, minimum of THD with success rate (Table 8) clearly proves that the proposed technique works effectively in contrast to other methods. Variations in passive components (resistors, inductors, capacitors) were introduced by applying ±5%–10% tolerance to nominal values. Power electronic switches were modeled with non-zero switching and conduction losses. Time delays were introduced in control signal transmission to emulate latency in real-time control environments or networked systems. Nonlinear and time-varying loads were used (e.g., diode bridge rectifiers, switching loads) to stress-test the control strategy under realistic disturbances. Besides, regarding the islanding scenario, UPQC is not traditionally used for intentional islanding detection. However, Real-time FLC and NNC inference still require a capable embedded platform (e.g., DSP or FPGA), which may add to hardware complexity.

Table 6: Comparison of % THD for all the cases with phases

Case	Controller/Ref. [ ]	%THD of source current		
		Phase-a	Phase-b	Phase-c
1	GA	3.41	4.01	3.72
	FFA	3.31	3.22	3.35
	Proposed 5L-FFOA-based UPQC	2.23	2.37	2.31
2	GA	3.28	3.17	3.66
	FFA	3.11	3.17	3.21
	Proposed 5L-FFOA-based UPQC	3.64	3.68	3.71
	ANFIS [16]	2.43	–	–
	FLC [16]	6.13	–	–
	PIC [16]	14.74	–	–
	BF tuned PIC [14]	3.71	–	–
	ACO tuned PIC [14]	3.72	–	–
	PIC [14]	3.88	–	–
	PSO [13]	2.09	–	–
	HSO [13]	2.41	–	–
	ZN [13]	7.57	–	–
	ICM [13]	4.2	–	–
3	GA	3.26	3.43	3.71
	FFA	2.41	2.54	2.24
	Proposed 5L-FFOA-based UPQC	2.21	2.27	2.24

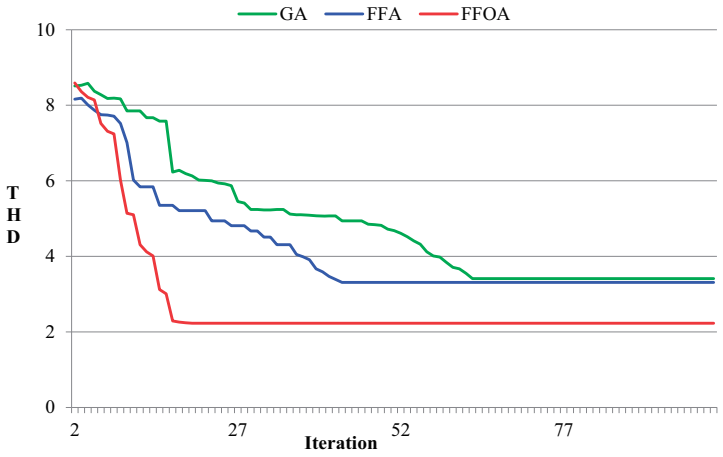

Figure 17: THD convergence for case-1 with proposed 5 Level FFOA with 5 Level GA and 5 Level FFA

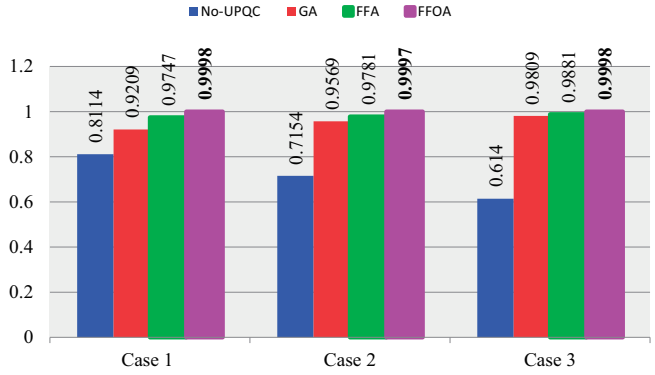

Figure 18: PF comparison for case studies

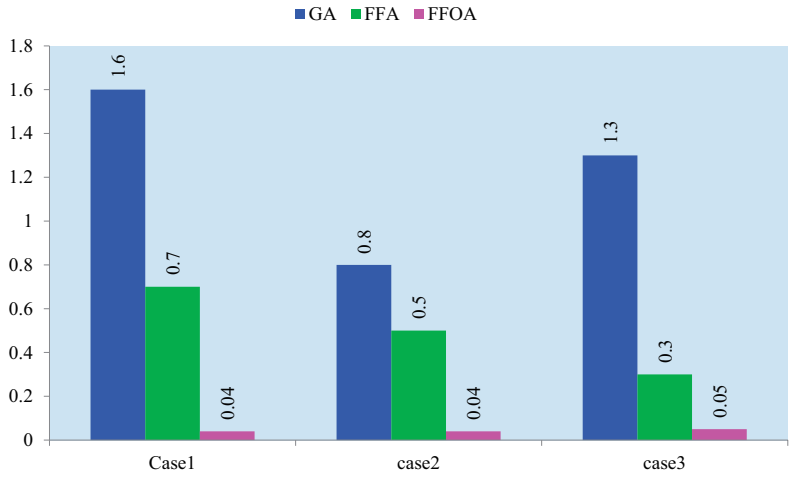

Figure 19: Comparison plot of time taken in sec to reach DC link capacitor voltage (DLCV) stable

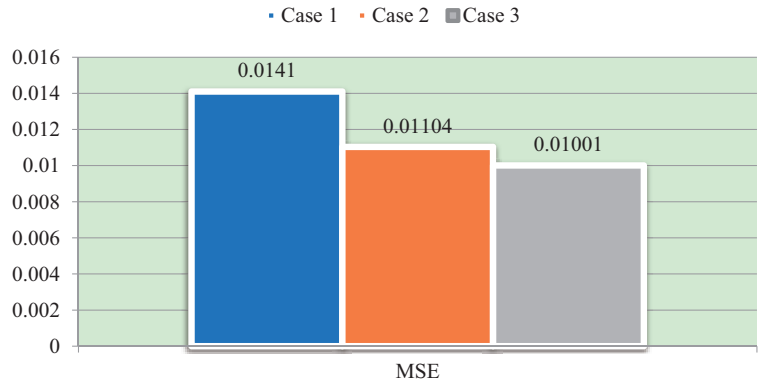

Figure 20: MSE for case studies

Table 7: Comparison of optimally selected design parameters for all the cases

Case	Method	R_{se}	R_{sh}	L_{se}	L_{sh}
1	GA	2.271	0.315	6.552	7.223
	FFA	8.542	0.654	2.355	5.245
	FFOA	**2.472**	**0.301**	**2.001**	**9.422**
2	GA	2.001	0.225	6.339	7.245
	FFA	1.005	0.346	1.002	4.102
	PIC [14]	–	–	–	–
	ACO tuned PIC [14]	–	–	–	–
	BF tuned PIC [14]	–	–	–	–
	PSO [13]	–	–	–	–
	HSO [13]	–	–	–	–
	ZN [13]	–	–	–	–
	ICM [13]	–	–	–	–
	ABC [17]	–	–	–	–
	GSA [17]	–	–	–	–
	FA [17]	–	–	–	–
	MFOA [17]	–	–	–	–
	FFOA	**6.335**	**0.364**	**1.993**	**4.898**
3	GA	6.998	0.214	2.457	5.541
	FFA	6.887	0.104	7.998	2.887
	FFOA	**8.445**	**0.336**	**1.225**	**7.998**

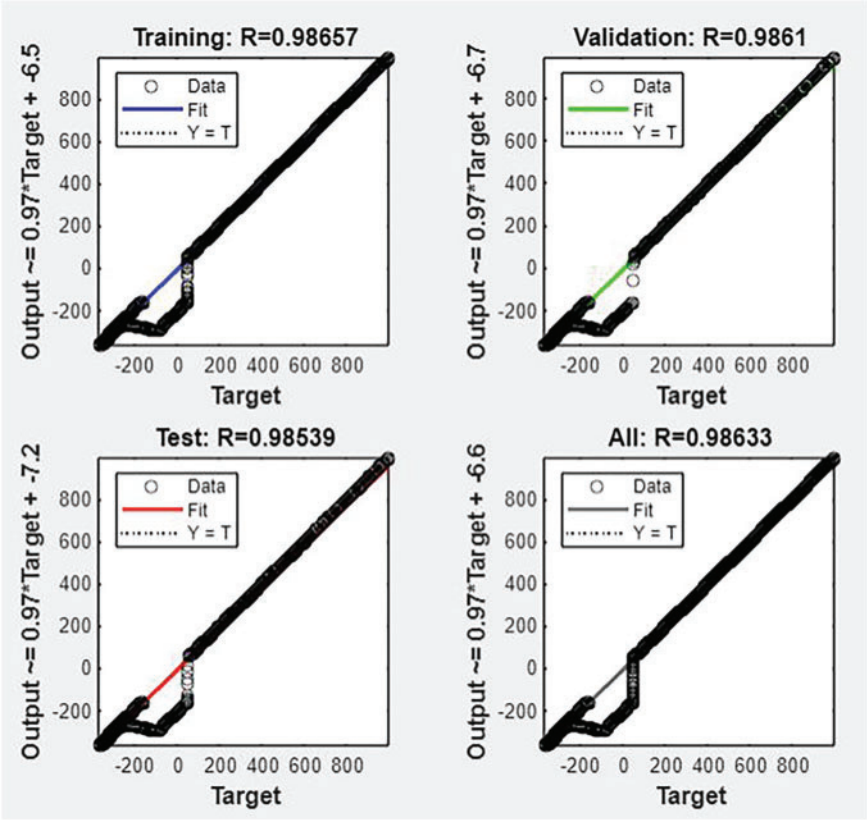

Figure 21: Regression Plot

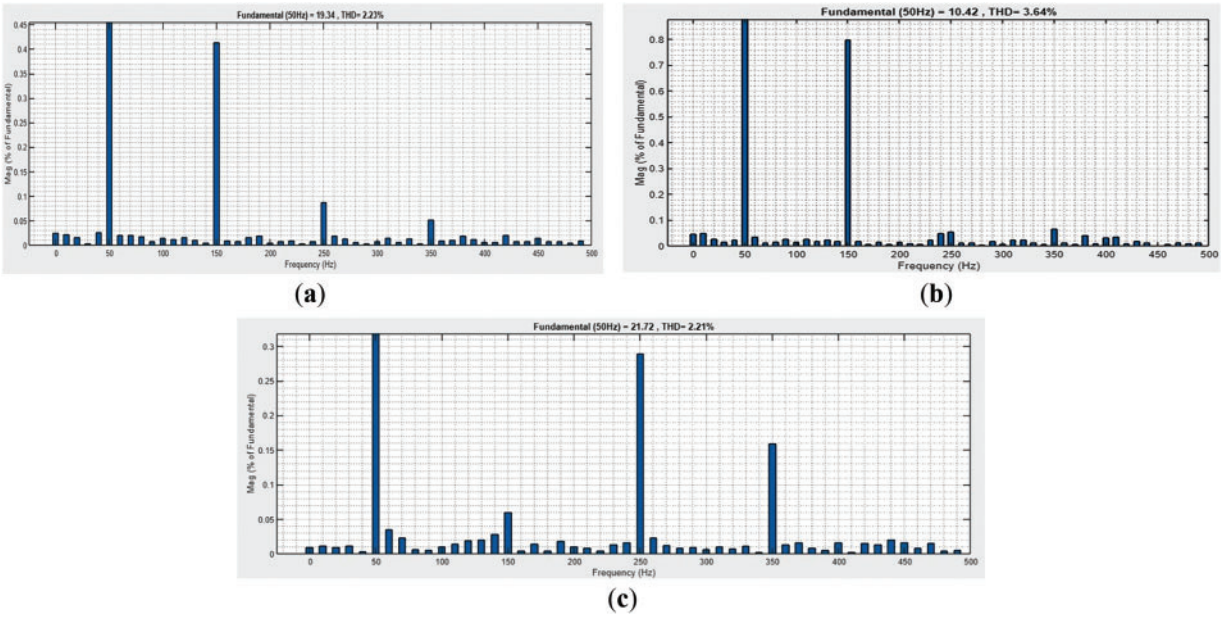

Figure 22: Current %THD spectrum for case studies. **(a)** Case-1; **(b)** Case-2; **(c)** Case-3

Table 8: Statistical comparison of THD result for case-1

Algorithm	%THD			% Rate of success
	Maximum value	Minimum value	Average	
GA	4.56	3.41	3.93	78
FFA	4.09	3.31	3.85	87
FFOA	2.87	2.23	2.88	92

6 Conclusion

A sophisticated fuzzy logic regulation is utilized to efficiently manage electricity in a system consisting of the Grid, RES, BESS, and EVs. UPQC is utilized to address PQ concerns to maintain a consistent DC link voltage under different load levels, wind velocities, and irradiation circumstances. Furthermore, the FFOA technique is utilized to train the NNC while simultaneously selecting suitable filter settings. The objective of the developed power management technique is to satisfy the load requirement and accommodate the necessary quantity of EVs. This study efficiently addresses both PQ issues and power management simultaneously. The device efficiently mitigates voltage fluctuations, swells, sags, and flaws in the current waveforms. Nevertheless, using this suggested methodology, the THD values for currents have been below 5%. Subsequent investigations may expand upon the findings of this work by using metaheuristic algorithms to further augment the efficacy of power flow regulation. However, the proposed method is effective to seven-level (and beyond) systems with enhanced control schemes, ensuring stable DC link voltages and reliable UPQC performance with hydrogen energy and future smart inverters.

Acknowledgement: Not applicable.

Funding Statement: The authors received no specific funding for this study.

Author Contributions: The authors confirm contribution to the paper as follows: Conceptualization, Praveen Kumar Balachandran and Koganti Srilakshmi; methodology, Vadla Babyshalini and Gudikandhula Kalpana; software, Subhav Singh; validation, Subhav Singh, Vadla Babyshalini and Gudikandhula Kalpana; formal analysis, Koganti Srilakshmi; investigation, Praveen Kumar Balachandran and Koganti Srilakshmi; resources, Praveen Kumar Balachandran; data curation, Subhav Singh, Vadla Babyshalini and Gudikandhula Kalpana; writing—original draft preparation, Praveen Kumar Balachandran and Koganti Srilakshmi; writing—review and editing, Vadla Babyshalini and Gudikandhula Kalpana; visualization, Subhav Singh; supervision, Praveen Kumar Balachandran; project administration, Praveen Kumar Balachandran and Subhav Singh; funding acquisition, Praveen Kumar Balachandran. All authors reviewed the results and approved the final version of the manuscript.

Availability of Data and Materials: The data that support the findings of this study are available from the corresponding author, Praveen Kumar Balachandran, upon reasonable request.

Ethics Approval: Not applicable.

Conflicts of Interest: The authors declare no conflicts of interest to report regarding the present study.

References

1. Elavarasan RM. Comprehensive review on India's growth in renewable energy technologies in comparison with other prominent renewable energy based countries. J Sol Energy Eng. 2020;3(142):1–11. doi:10.1115/1.4045584.
2. Madurai Elavarasan R, Afridhis S, Vijayaraghavan RR, Subramaniam U, Nurunnabi M. SWOT analysis: a framework for comprehensive evaluation of drivers and barriers for renewable energy development in significant countries. Energy Rep. 2020;6(10):1838–64. doi:10.1016/j.egyr.2020.07.007.
3. Madurai Elavarasan R, Selvamanohar L, Raju K, Vijayaraghavan RR, Subburaj R, Nurunnabi M, et al. A holistic review of the present and future drivers of the renewable energy mix in Maharashtra state of India. Sustainability. 2020;16(12):6596. doi:10.3390/su12166596.
4. Shafiullah GM, Arif MT, Oo AMT. Mitigation strategies to minimize potential technical challenges of renewable energy integration. Sustain Energy Technol Assess. 2018;25:24–42. doi:10.1016/j.seta.2017.10.008.
5. Ashok Kumar L, Indragandhi V. Power quality improvement of grid connected wind energy system using facts devices. Int J Ambient Energy. 2020;6(41):631–40. doi:10.1080/01430750.2018.1484801.
6. Mohamed SA. Enhancement of power quality for load compensation using three different FACTS devices based on optimized technique. Int Trans Electr Energy Syst. 2020;3(30):12196. doi:10.1002/2050-7038.12196.
7. Paramanik S, Sarker K, Chatterjee D, Goswami SK. Smart grid power quality improvement using modified UPQC. In: 2019 Devices for Integrated Circuit (DevIC); 2019 Mar 23–24; Kalyani, India. p. 356–60.
8. Nunes P, Brito MC. Displacing natural gas with electric vehicles for grid stabilization. Energy. 2017;141(2):87–96. doi:10.1016/j.energy.2017.09.064.
9. Kong PY, Karagiannidis GK. Charging schemes for plug-in hybrid electric vehicles in smart grid: a survey. IEEE Access. 2016;4:6846–75. doi:10.1109/access.2016.2614689.
10. Chellaswamy C, Ramesh R. Future renewable energy option for recharging full electric vehicles. Renew Sustain Energy Rev. 2017;76(4):824–38. doi:10.1016/j.rser.2017.03.032.
11. Amirullah A, Ananda A, Penangsang O, Soeprijanto A. Load active power transfer enhancement using UPQC-PV-BES system with fuzzy logic controller. Int J Intell Eng Syst. 2020;2(13):329–49.
12. Vivas FJ, Segura F, Andújar JM, Palacio A, Saenz JL, Isorna F, et al. Multi-objective fuzzy logic-based energy management system for microgrids with battery and hydrogen energy storage system. Electronics. 2020;7(9):1074. doi:10.3390/electronics9071074.
13. Mahaboob S, Ajithan SK, Jayaraman S. Optimal design of shunt active power filter for power quality enhancement using predator-prey based firefly optimization. Swarm Evol Comput. 2019;44(5):522–33. doi:10.1016/j.swevo.2018.06.008.
14. Sakthivel A, Vijayakumar P, Senthilkumar A, Lakshminarasimman L, Paramasivam S. Experimental investigations on ant colony optimized pi control algorithm for shunt active power filter to improve power quality. Control Eng Pr. 2015;42(3):153–69. doi:10.1016/j.conengprac.2015.04.013.
15. Nagireddy VV, Kota VR, Ashok Kumar DV. Hybrid fuzzy back-propagation control scheme for multilevel unified power quality conditioner. Ain Shams Eng J. 2018;9(4):2709–24. doi:10.1016/j.asej.2017.09.004.
16. Renduchintala UK, Pang C, Tatikonda KM, Yang L. ANFIS-fuzzy logic based UPQC in interconnected microgrid distribution systems: modeling, simulation and implementation. J Eng. 2021;21(1):1–29. doi:10.1049/tje2.12005.
17. Rajesh P, Shajin FH, Umasankar L. A novel control scheme for PV/WT/FC/Battery to power quality enhancement in micro grid system: a hybrid technique. Energy Sources Part A Recov Util Env Eff. 2021;47(1):9126–42. doi:10.1080/15567036.2021.1943068.

18. Ganesan A, Subbaraman S. Optimal controller for mitigation of harmonics in hybrid shunt active power filter connected distribution system: an EGOANN technique. J Renew Sustain Energy. 2019;11(2):025507. doi:10.1063/1.5085028.
19. Xiaojun Z, Xiuhui C, Xiaoqiang G, Ahmad W, Xiaohuan W, Chunjiang Z. Impedance matching-based power flow analysis for UPQC in three-phase four-wire systems. Energies. 2021;14(9):2702. doi:10.3390/en14092702.
20. Mansoor MA, Hasan K, Othman MM, Noor SZBM, Musirin I. Construction and performance investigation of three phase solar PV and battery energy storage system integrated UPQC. IEEE Accesses. 2020;8:103511–38. doi:10.1109/access.2020.2997056.
21. Okwako OE, Lin ZH, Xin M, Premkumar K, Rodgers AJ. Neural network controlled solar PV battery powered unified power quality conditioner for grid connected operation. Energies. 2022;15(18):6825. doi:10.3390/en15186825.
22. Trojovská E, Dehghani M, Trojovský P. Fennec fox optimization: a new nature-inspired optimization algorithm. IEEE Access. 2022;10(4):84417–43. doi:10.1109/access.2022.3197745.
23. Sarita S, Prakash KH, Qingsong A. Design and analysis of solar PV-fuel cell and wind energy based microgrid system for power quality improvement. Cogent Eng. 2017;4(1):1402453. doi:10.1080/23311916.2017.1402453.
24. Kesler M, Ozdemir E. Synchronous-reference-frame-based control method for UPQC under unbalanced and distorted load conditions. IEEE Trans Ind Electron. 2011;58(9):3967–75. doi:10.1109/tie.2010.2100330.
25. Srilakshmi K, Sujatha CN, Balachandran PK, Mihet-Popa L, Kumar NU. Optimal design of an artificial intelligence controller for solar-battery integrated UPQC in three phase distribution networks. Sustainability. 2022;14(21):13992. doi:10.3390/su142113992.
26. Srilakshmi K, Kondreddi K. Optimal design of hybrid green energy powered reduced switch converter based shunt active power filter using horse herd algorithm. Sci Rep. 2024;14:20447.
27. Srilakshmi K, Santosh DT, Ramadevi A, Balachandran PK, Reddy GP, Palanivelu A, et al. Development of renewable energy fed three-level hybrid active filter for EV charging station load using Jaya grey wolf optimization. Sci Rep. 2024;14(1):4429. doi:10.1038/s41598-024-54550-7.
28. Srilakshmi K, Kumar A, Kondreddi K, Krishna TM, Balachandran PK, Gatto G. Design of solar and energy storage systems fed reduced switch multilevel converter with flower pollination optimization. J Energy Storage. 2024;99(Pt A):113324. doi:10.1016/j.est.2024.113324.
29. Belqasem A, Yaswanth A, Srilakshmi K, Praveen B, Sudhakar T. An optimized neural network-honey badger based control technique for a hybrid solar PV and battery energy storage fed unified power quality conditioner. J Energy Storage. 2025;106(8):114818. doi:10.1016/j.est.2024.114818.
30. Zaidi S, Meliani B, Riyadh B, Habib B, Saad M, Elbarbary ZMS. Intelligent control of hybrid energy storage system using NARX-RBF neural network techniques for microgrid energy management. Energy Rep. 2024;12(9):5445–61. doi:10.1016/j.egyr.2024.11.023.